Available online at www.sciencedirect.com
ScienceDirect
Journal of the European Ceramic Society 30 (2010) 1989–2001
www.elsevier.com/locate/jeurceramsoc

Calcium carbonate thermal decomposition in white-body wall tile during firing. I. Kinetic study

A. Escardino *, J. García-Ten, C. Feliu, A. Moreno

Instituto de Tecnología Cerámica, Asociación de Investigación de las Industrias Cerámicas, Universitat Jaume I, Castellón, Spain

Received 17 November 2009; received in revised form 17 March 2010
Available online 6 May 2010

Abstract

This study examines the thermal decomposition of calcium carbonate, contained in disk-shaped test pieces formed from a mixture of raw materials of a similar composition and characteristics to those of the mixtures customarily used for the manufacture of white-body wall tile.

The experiments were conducted under isothermal conditions at different temperatures in the range 825–950 °C in an air stream free of carbon dioxide.

The experimental results have been interpreted using the Shrinking Unreacted Core kinetic model, assuming that, at low conversion degrees, the process is only controlled by the chemical reaction step of $CaCO_3$ decomposition, while at high conversion degrees the diffusion of the resulting CO_2 through the porous structure of the reacted ceramic layer also affects the process. The derived equations, which relate the conversion degree of calcium carbonate in the ceramic body to residence time, temperature, and initial porosity of the test pieces, allow the experimental results to be satisfactorily reproduced.

Keywords: Calcination; Traditional ceramics

1. Introduction

The raw materials mixture used to make wall tile bodies typically contains 8–15% calcium carbonate (by weight) which, on decomposing during firing, provides the calcium oxide required to produce certain crystalline phases, usually involving calcium silicates and aluminosilicates (gehlenite, anorthite, and wollastonite). These crystalline phases form at temperatures above 870 °C as a result of the reaction of CaO with Al_2O_3 and SiO_2 stemming from the decomposition of the clay minerals present in the starting raw materials mixture.[1–3]

The clays used to fabricate white-firing bodies usually contain no carbonates, so that an appropriate quantity of calcite particles (with an average radius of 3.5 μm,) is usually added as a source of CaO, calcite being cheaper than other calcium-containing minerals, such as wollastonite.[4,5]

In this process, the uniformly distributed small calcite particles in the green body need to decompose during firing between 800 and 950 °C.

The calcite particles decompose above 600 °C during the firing stage, releasing carbon dioxide, according to the following reversible reaction[6]:

$$CaCO_3(s) \leftrightarrow CaO(s) + CO_2(g)$$

This reversible chemical reaction may be expressed, using the generalised nomenclature, by the following reaction scheme:

$$-\nu_B B(s) = \nu_P P(s) + \nu_Q Q(g) \quad (1)$$

where $B = CaCO_3$, $P = CaO$, $Q = CO_2$, and $-\nu_B = \nu_P = \nu_Q = 1$.

In the firing cycle, this reaction needs to end before the glaze sealing temperature (i.e. the temperature at which the molten glaze fully covers the body) is reached, to prevent the carbon dioxide that is being liberated in the body from being trapped as small bubbles in the molten glaze, and producing various defects in the outer surface of the end product.[7] This decomposition reaction therefore usually takes place in the 825–950 °C temperature range in industrial practice.

The time needed to decompose the calcite in the ceramic body, during industrial firing, is usually empirically determined. It was considered of interest, therefore, to obtain a mathematical expression that would relate the progress of the thermal decom-

* Corresponding author.
E-mail address: aescardino@itc.uji.es (A. Escardino).

0955-2219/$ – see front matter © 2010 Elsevier Ltd. All rights reserved.
doi:10.1016/j.jeurceramsoc.2010.04.014

Nomenclature

c_B^0 initial molar concentration of $CaCO_3$ in the test disk (kmol/m^3)
c_Q^G molar concentration of CO_2 in the gas phase (kmol/m^3)
c_{QS}^G molar concentration of CO_2 at the gas–solid interface, gas side (kmol/m^3)
c_{Qe}^S molar concentration of CO_2 in equilibrium with the solid at temperature T of the particle (kmol/m^3)
c_{Qi}^S molar concentration of CO_2 at the reaction interface (kmol/m^3)
c_{QS}^S molar concentration of CO_2 at the gas–solid interface, solid side (kmol/m^3)
D_e effective overall diffusivity of CO_2 through the reacted layer (m^2/min)
D_y intergrain diffusion coefficient of CO_2 through the reacted layer of thickness Y (m^2/min)
D_0 pre-exponential factor of Eq. (18)
E_D apparent activation energy of Eq. (18)
k rate constant of the direct reaction (kmol/(m^2 min) in Eq. (3)
K_c equilibrium constant (kmol/m^3) in Eq. (3)
k_G mass transfer coefficient (m/min)
L test disk initial thickness (m)
N_B^0 initial moles of $CaCO_3$ in the test disk (kmol)
N_B moles of $CaCO_3$ in the test disk after time t has elapsed (kmol)
P_Q^0 decomposition pressure of calcium carbonate at temperature T (atm)
R gas constant (8.314 J mol^{-1} K^{-1} or 0.082 atm m^3 kmol^{-1} K^{-1})
R_j decomposition reaction rate in reference to A_j (kmol A$_j$/min); ($A_j = B$, Q, P)
S_i reaction interface area (m^2)
S_s cross-sectional area of the test piece (m^2)
t reaction time (min)
T temperature (K)
v_G linear velocity of the gas through the reactor (m^3/s)
V_B^0 initial volume of the test disk (m^3)
W_Q^S CO_2 overall flow rate from the reaction interface to the solid–gas interface (kmol CO_2/min)
$(W_Q^S)_{dif}$ CO_2 flow rate by intergrain diffusion from the reaction interface to the solid–gas interface (kmol CO_2/min)
$(W_Q^S)_{v_f}$ CO_2 flow rate by viscous flow from the reaction interface to the solid–gas interface (kmol CO_2/min)
W_Q^G CO_2 flow rate from the solid–gas interface to the gas phase (kmol CO_2/min)
X $CaCO_3$ degree of conversion calculated from Eq. (2)
Y thickness of the reacted layer (m)
Δm_B mass loss of B in the sample at a given reaction time (t) (min)
Δm_{Bf} mass loss of B in the sample at a sufficiently long time to achieve constant weight, when all calcium carbonate is assumed to have decomposed

Greek letters
ρ_B^0 initial molar density of $CaCO_3$ in the test disk (kmol B/m^3 test disk)
υ_B, υ_Q, υ_P stoichiometric coefficients of $CaCO_3$, CO_2, and CaO in Eq. (1)
ε_0 initial porosity
μ_Q CO_2 viscosity (kg/(m min))

Table 1
Composition of the raw materials mixture used.

Raw material	Content (% by weight)
Clay	60
Feldspathic sand	25
Calcite	15

position process of the small calcite particles contained in the initial mass of the body, to the main operating variables (time, temperature, body porosity, etc.) in order to be able to calculate the most appropriate time and temperature range for this process to unfold in industrial practice.

2. Materials and experimental procedure

2.1. Materials

The present study was conducted with test pieces formed from the mixture of natural raw materials detailed in Table 1. This composition and these types of raw materials are customarily used in the ceramic industry for manufacturing wall tile bodies. The chemical composition of the raw materials used is given in Table 2. The calcite particles used to

Table 2
Chemical composition, expressed in % by weight of oxides, of the raw materials used.

Oxide	Clay	Feldspathic sand	Calcite
SiO_2	64.6	88.5	0.2
Al_2O_3	22.1	6.5	0.1
Fe_2O_3	2.11	0.15	0.05
TiO_2	1.10	0.08	–
Na_2O	0.15	0.13	–
K_2O	2.00	2.84	0.01
CaO	0.23	0.17	55.7
MgO	0.28	<0.01	0.20
P_2O_5	0.10	0.02	0.11
MnO	0.01	–	0.01
L.O.I.	7.20	1.54	43.5

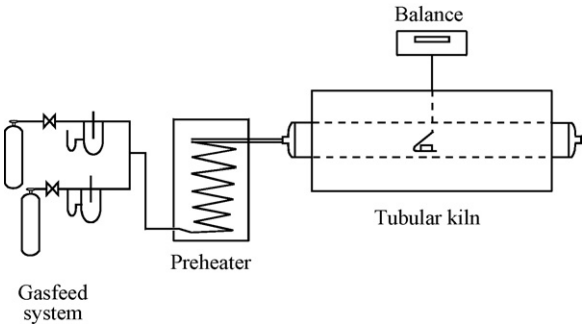

Fig. 1. Experimental assembly.

prepare the raw materials mixture had an average radius of 3.5 μm.

2.2. Experimental assembly

The calcium carbonate decomposition reaction during firing was monitored by measuring sample weight loss during isothermal treatment in a laboratory tubular kiln. Air was fed into the kiln at a controlled temperature and speed. Fig. 1 schematically illustrates the experimental assembly used. The assembly consisted of a refractory steel sample-holder, set in the middle of the kiln firing chamber. The holder was suspended from a single-pan balance by an alumina rod, so that sample mass could be continuously measured. The balance was connected to a computer with the appropriate software to record the pairs of mass–time values.

2.3. Experimental procedure

The raw materials mixture detailed in Tables 1 and 2 was used to prepare cylindrical test pieces, 40 mm in diameter and 7 mm thick, by uniaxial pressing. Pressing powder moisture content was kept constant at 0.055 kg water/kg dry solid and the pressure applied was modified to obtain test pieces with different dry bulk densities. The test pieces were preheated for 30 min, in CO_2 atmosphere, in an oven that ran at a temperature close to that of the pre-set operating temperature. The side of each test piece was sealed with a glaze to prevent any lateral CO_2 losses during thermal treatment, so that CO_2 would only be released through the two faces of the disk.

The experiments were conducted under isothermal conditions, at six different temperatures (825, 850, 875, 900, 925, and 950 °C), in an air stream free of carbon dioxide. For this purpose, the reactor and preheater resistances were switched on first, and the desired operating temperature set. The airflow rate into the reactor was then adjusted.

Once the chosen temperature had been reached, the data logging system was switched on, the test piece was withdrawn from the oven and rapidly placed in the reactor, where the mass–time pairs of values were recorded. Reaction time continued until the test piece mass stabilised. The piece was then withdrawn from the reactor.

3. Experimental results

3.1. Determination of the calcium carbonate degree of conversion during thermal treatment of the test pieces

When wall tile bodies are fired, a further series of decomposition reactions occur in addition to calcium carbonate decomposition, with the ensuing mass losses. Those reactions include dehydroxylation of the clay minerals used to form the body, together with calcite, and oxidation of the organic matter that those components usually contain. The mass loss of the test pieces, determined by the experimental procedure described in Section 2.3, is thus due to the sum of all those transformations, which may be represented by the following overall reaction scheme:

$$A(\mathrm{s}) + B(\mathrm{s}) \Rightarrow P(\mathrm{s}) + Q(\mathrm{g}) + S(\mathrm{s}) + R(\mathrm{g})$$

where A represents the clay, feldspathic sand, and organic matter, and B the calcite ($CaCO_3$) initially contained in the test piece; P represents the CaO that forms; Q the CO_2 that is released; and S and R the (solid and gaseous) decomposition reaction products of the clay–feldspathic sand mixture.

The results of the simultaneous thermal analysis of the clay and feldspathic sand used in this study indicated that the temperature range in which the dehydroxylation of these materials took place began around 370 °C, with mass loss continuing up to temperatures above 800 °C. As a result, the calcite decomposition reaction, which began at about 600 °C, partly overlapped the decomposition reactions of the clay–feldspathic sand mixture used, together with the calcite, to make the test pieces with which the study was conducted.

In order only to obtain the mass loss curves for calcium carbonate particle decomposition in the test pieces (Δm_B), it was necessary to perform two series of experiments in each case. In one series, the test pieces were formed from the mixture of clay, feldspathic sand, and calcite ($A - B$) and, in the other, from the same mixture of clay and feldspathic sand (same quantities) without calcite (A).

The series of experiments conducted with test pieces formed with the clay, feldspathic sand, and calcite mixture yielded the curve $\Delta m_{A-B(t)} = m_{A-B0} - m_{A-B(t)} = f(t)$, of total mass loss with reaction time, where m_{A-B0} is the initial test piece mass and $m_{A-B(t)}$ is the test piece mass measured at different reaction times. In each case, $\Delta m_{A-Bf} = m_{A-B0} - m_{A-Bf}$ was determined at the reaction time where no further mass loss was observed in the test piece.

The same operation was performed in the series of experiments conducted with test pieces formed with the clay and feldspathic sand mixture without calcite, which contained the same quantity and the same initial mass (m_{A0}) of these components as the test piece mentioned in the foregoing paragraph. This yielded the decomposition curve $\Delta m_{A(t)} = m_{A0} - m_{A(t)} = f(t)$. In this case, $m_{A(t)}$ is the test piece mass that corresponds to any reaction time (t). The test was also continued until the mass remained practically constant (m_{Af}), with a view to calculating $\Delta m_{Af} = m_{A0} - m_{Af}$.

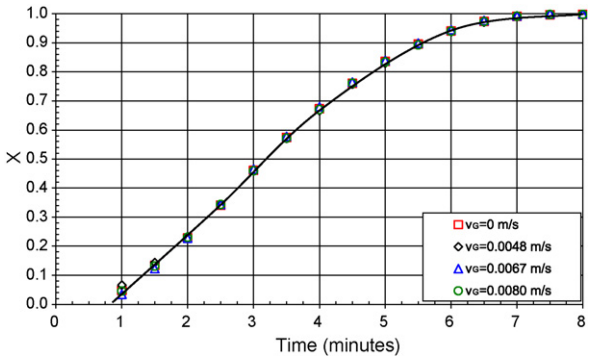

Fig. 2. Evolution of $CaCO_3$ degree of conversion with reaction time for the different tested v_G values.

With the values of m_{A-B0}, m_{A0}, m_{A-Bf}, and m_{Af}, and the pairs of values of $m_{A(t)}$ and $m_{A-B(t)}$ obtained for each reaction time, in each experiment, the conversion degree (X) of the $CaCO_3$ content in the test piece was calculated from the expression:

$$X = \frac{\Delta m_B}{\Delta m_{Bf}} = \frac{m_{B0} - m_B}{m_{B0} - m_{Bf}} = \frac{(m_{A-B0} - m_{A-B}) - (m_{A0} - m_A)}{(m_{A-B0} - m_{A-Bf}) - (m_{A0} - m_{Af})} \quad (2)$$

Minimum gas velocity through the reactor at which the CO_2 mass transfer step from the test piece surface to the gas phase does not influence the overall process rate

In order to determine the gas (air) linear velocity through the reactor (v_G) at which the CO_2 transfer step from the surface of the test pieces into the gas phase no longer influences the overall process rate, several experiments were conducted, maintaining all operating conditions constant except gas velocity through the reactor.[8,9]

In these experiments, 7-mm-thick test pieces with a dry bulk density of 1850 kg/m^3 ($\varepsilon_0 = 0.304$) were subjected to isothermal heat treatment at 950 °C. These were the operating conditions under which, in principle, the decomposition reaction and carbon dioxide diffusion rates through the structure of the piece were highest in the studied temperature range and under which, therefore, the mass transfer rate between the surface of the piece and the gas phase could be expected most readily to influence the overall process rate in the temperature range to be tested. The results obtained have been plotted in Fig. 2.

It may be observed in this figure that the curves of conversion degree versus time coincide in the entire studied v_G range. These findings indicate that, at very low gas velocities, the mass transfer step between the test piece surface and the gas phase is already much faster than the other process steps, the operating conditions therefore not influencing the overall process rate, under the operating conditions used in the tests described below.

In view of the above, all the experiments that were subsequently conducted, whose results are set out in the following sections, were designed such that v_G was 0.0067 m/s or higher.

3.2. Programming of experiments and results obtained

In order to select a representative kinetic model of the decomposition process mechanism of the calcite contained in the test pieces formed with the raw materials mixture used (Table 1), with a view to having equations that related the degree of process progress to the different operating variables and to reaction time, several series of experiments were planned. Each experiment would be conducted under constant operating conditions (temperature, composition of the gas phase, calcite content of the test pieces, test piece thickness, etc.), X being determined at different reaction times and one of the following operating variables being modified in each series of experiments: temperature and/or compactness or porosity of the piece. Reaction time would begin to be counted from the moment the test piece was placed in the reactor running at the desired reaction temperature.

Eighteen series of three experiments were conducted, using 7.0-mm-thick test pieces, 40 mm in diameter, containing 15.0% (by weight) calcite particles, with an average radius of 3.5 μm. The gas phase used in all experiments was an air stream with a negligible CO_2 partial pressure.

Six temperatures were tested: 825, 850, 875, 900, 925, and 950 °C, for three test piece bulk densities: 1850, 1950, and 2050 kg/m^3 (corresponding, respectively, to initial dry porosities of 0.304, 0.267, and 0.229 and to initial molar densities of 2.775, 2.925, and 3.075 kmol of calcium carbonate/m^3 test piece).

The experimental results obtained have been plotted in Figs. 8–13, in the form conversion degree of the calcium carbonate contained in the test pieces (X) versus reaction time (t).

4. Discussion of results

4.1. Kinetic model

The following may be observed in the plots of the experimental data $X = f(t)$ in Figs. 8–13:

(a) At each test temperature, there is a section, in the region of the lowest conversion degrees, in which the curves corresponding to the three green bulk densities (initial porosities) of the test pieces have practically coinciding paths (the curve slope decreases slightly at every test temperature when calcium carbonate molar density increases). This section, which comprises the conversion degrees (X) from 0.0 to 0.5 at the lowest test temperature of 825 °C, increases as the operating temperature rises, and practically includes the entire range of values of this composition variable at the studied peak temperature (950 °C).

(b) In the curve sections corresponding to the highest ranges of X values, the reduction in test piece initial porosity reduces the slope of the $X = f(t)$ curves, which shift towards the x-axis.

In view of these results, and by analogy with previous studies,[10,11] it was decided to attempt to correlate the experimen-

tal results with the *Shrinking Unreacted Core kinetic model*[12,13] since this seemed qualitatively to match the behaviour described in the foregoing paragraphs.

In effect, this model can explain the curve behaviour observed in the sections of the lowest conversion degrees when, in that range of X values, the chemical reaction step of calcium carbonate decomposition unfolds at a much slower rate than the carbon dioxide diffusion step through the structure of the reacted ceramic layer of the test piece, which is why it could be the overall process rate controlling step. According to the *Shrinking Unreacted Core kinetic model*, at short reaction times, the thickness of the shell in which the calcite ($CaCO_3$) has decomposed is either zero (when the decomposition process begins at the surface and moves inwards into the test piece) or very small, so that it is quite reasonable for the CO_2 diffusion step through the test piece to unfold at a greater rate than the chemical reaction step. This would explain the practical coincidence of the three curves corresponding to the different initial porosities at short residence times and the lowest conversion ranges.

In contrast, at highest conversion degrees, since the shell mentioned becomes quite thick, the CO_2 diffusion step through the test piece can already influence the overall process rate, together with the chemical reaction step. In this case, when test piece initial porosity decreases, the directly related effective diffusivity[11,14–17] must become smaller, hence also reducing the slope of the curve as the plots in Figs. 8–13 show.

The fact that at 925 and 950 °C (Figs. 8–13) the last sections of the three $X=f(t)$ curves, obtained at the three tested degrees of porosity, lie close together in the entire range of X values might stem from the fact that, at temperatures above 900 °C, calcium carbonate decomposition pressure exceeds the atmospheric pressure at which the reactor operates, causing CO_2 transport through the porous structure of the shell to occur by laminar flow, as well as by diffusion, because of the static pressure gradient that develops. As a result, the CO_2 flow rate through this shell must be higher than that which would occur if the sole transport mechanism were by diffusion, leading to higher effective diffusivity values than expected.

It was decided, therefore, to test the *Shrinking Unreacted Core kinetic model*, applied to flat slabs of finite thickness and infinite width and length, even though the test pieces used in the study were 7-mm-thick disks, 40 mm in diameter, whose sides were sealed to prevent or reduce lateral CO_2 losses.

In order to deduce the corresponding $X=f(t)$ equation, the following reaction rate equation was used for the calcite chemical decomposition step in the test pieces[18,20]:

$$R_B = (1-X)^{1/3} S_i k \left(1 - \frac{C_{Qi}^S}{K_C}\right) \tag{3}$$

where R_B is expressed in kmol B/(min), S_i (reaction interface area) in m^2, k in kmol/(min m^2), K_C (equilibrium constant) in kmol/m^3. In this expression, c_{Qi}^S represents the CO_2 molar concentration at the reaction interface and X is the calcium carbonate conversion degree.

Since the resistance corresponding to the CO_2 transfer step from the test piece surface to the gas phase by turbulent transport is negligible, as noted above, because sufficiently high gas velocities through the reactor were used in all experiments (Section 3.2), the overall process rate must be solely controlled by the chemical reaction and diffusion steps. The $X=f(t)$ equation indicated above therefore adopts the form (Appendix A, Eq. (A.17)):

$$\frac{dX}{dt} = \left(\frac{1}{Lc_B^0}\right)\left[\frac{1 - c_Q^G/K_C}{S_S/kS_i(1-X)^{1/3} + LX/4D_eK_C}\right] \tag{4}$$

where S_i, k and K_C have been defined above and, X = degree of conversion of the calcite contained in the test piece determined from Eq. (2); (kmol of reacted calcite/kmol of calcite initially contained in the test piece), L = thickness of the test pieces (m), c_B^0 = initial calcite molar concentration in the test pieces (kmol calcium carbonate/m^3), S_S = cross-sectional area of the test piece (m^2), and D_e = effective diffusivity of carbon dioxide through the porous structure of the test pieces (m^2/min).

This equation can be analytically integrated from the initial boundary conditions ($X=0$, t_0), where t_0 is the real initial time as a result of the induction period (calculated in each series of experiments from the experimental data, given further below), yielding:

$$t = t_0 + \frac{3S_S L K_C c_B^0}{2kS_i(K_C - c_Q^G)}\left[1-(1-X)^{2/3}\right] + \frac{L^2 c_B^0 X^2}{8D_e(K_C - c_Q^G)} \tag{5}$$

When the chemical reaction step of calcium carbonate decomposition unfolds much more slowly than the CO_2 diffusion step and is, therefore, the sole overall process rate controlling step, in Eq. (4) the second term of the denominator of the expression in the second member bracket, which corresponds to the resistance opposed by the CO_2 diffusion step, can be disregarded, yielding the expression:

$$\frac{dX}{dt} = \left(\frac{1}{Lc_B^0}\right)\left[\frac{1 - c_Q^G/K_C}{S_S/kS_i(1-X)^{1/3}}\right] \tag{6}$$

This equation can also be analytically integrated from the initial boundary conditions ($X=0$, t_0), yielding:

$$t = t_0 + \frac{3S_S L K_C c_B^0}{2kS_i(K_C - c_Q^G)}\left[1-(1-X)^{2/3}\right] \tag{7}$$

4.2. Application of the proposed kinetic model to correlate the experimental results

4.2.1. First part of the experimental $X=f(t)$ data

In view of the shape of the graphs obtained when the experimental results were plotted, it was assumed that, for the lowest range of conversion degrees ($X<0.5$), the process might be controlled by the chemical reaction step, as suggested in Section 4.1. If this assumption is valid and the proposed kinetic model is appropriate, Eqs. (6) or (7) should fit the experimental data in this range of conversion degrees.

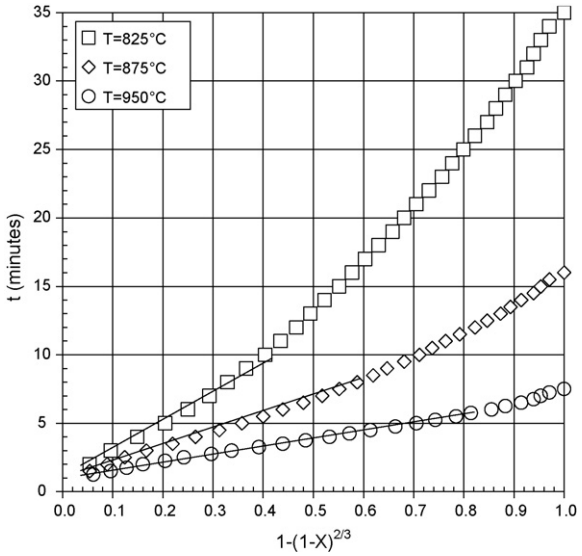

Fig. 3. Variation of reaction time (t) with $[1-(1-x)^{2/3}]$ at 825, 875, and 950 °C for test pieces with $\varepsilon_0 = 0.304$.

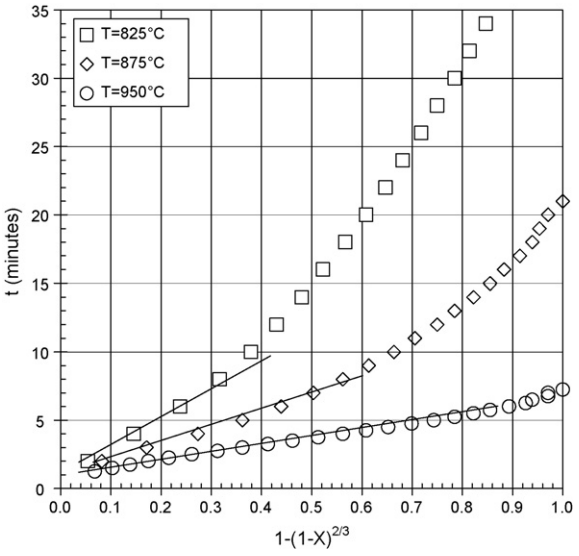

Fig. 4. Variation of reaction time (t) with $[1-(1-x)^{2/3}]$ at 825, 875, and 950 °C for test pieces with $\varepsilon_0 = 0.267$.

Since the experiments were conducted in the presence of an air stream practically without carbon dioxide, in order to attempt to correlate the experimental results of $X = f(t)$ it was necessary to set c_Q^G equal to zero in Eqs. (4)–(7). Eqs. (6) and (7) yield:

$$\frac{dX}{dt} = \frac{kS_i(1-X)^{1/3}}{Lc_B^0 S_S} \tag{8}$$

$$t = t_0 + \frac{3S_S Lc_B^0}{2kS_i}\left[1-(1-X)^{2/3}\right] \tag{9}$$

In accordance with Eq. (9), when the experimental data are plotted on rectangular coordinates, in the form t versus $[1-(1-X)^{2/3}]$, an ordinate straight line in the origin t_0, of slope $3S_S Lc_B^0/2kS_i$, should be obtained, if the starting assumptions are allowable.

When these plots were made, for all the conducted series of experiments, positive ordinate straight lines in the origin, of positive slope, were obtained at low residence times and $[1-(1-X)^{2/3}]$ corresponding to conversion degrees below 0.5. Figs. 3–5 display plots in the form mentioned, by way of example, of the experimental results obtained at 825, 875, and 950 °C. They show that when the temperature rises, the length of the straight stretch in these plots increases, i.e. the range of conversion degrees that they fit.

The results obtained appear to confirm the validity of Eqs. (8) and (9) for correlating the experimental results in the lowest range of conversion degrees.

Since the values of the variables L, S_S, and c_B^0 were known for each experiment, the values of the product (kS_i) and t_0 in Eq. (9), at each temperature and ε_0 conditions, could be determined from the value of the slope and the ordinate in the origin of the corresponding straight stretch. These values were confirmed when Eq. (8) was integrated with the fourth-order Runge–Kutta method starting at $X = 0$, trying different values of the product (kS_i) and of t_0 until the best fit was found.

The values of the product (kS_i) were determined instead of those of k, because the interface surface area (S_i) corresponding to the chemical reaction step was not precisely known.

Table 3 details the values of t_0 and of the product (kS_i) from the best fits obtained, corresponding to the first sections (straight stretch) of the plots resulting from the application of Eq. (9) to the experimental data. The value of t_0 (induction time of each experiment) ranged from 0.7 to 1.1 min, depending on the operating temperature and initial porosity of the studied piece.

4.2.2. *Second part of the experimental $X = f(t)$ data*

Using the values of the product (kS_i) and of t_0 detailed in Table 3, calculated in the form indicated, Eq. (5) was then applied to the entire range of experimental data $X = f(t)$, in each series of

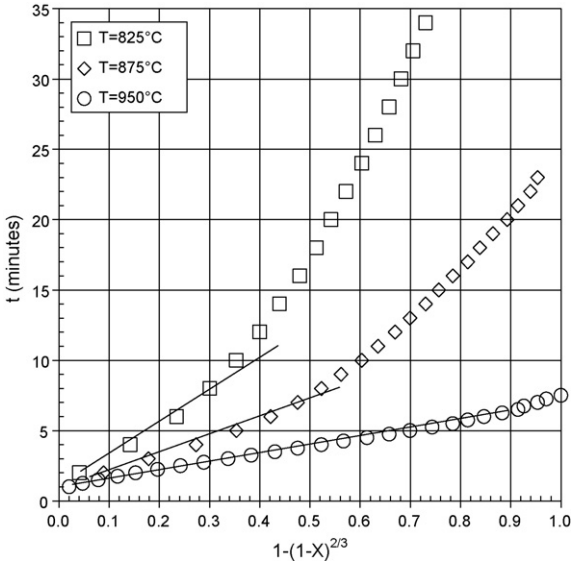

Fig. 5. Variation of reaction time (t) with $[1-(1-x)^{2/3}]$ at 825, 875, and 950 °C for test pieces with $\varepsilon_0 = 0.229$.

Table 3
Values of t_0 and of product kS_i obtained in the best fits with Eq. (9); ($L = 0.007$ m; $S_s = 0.00125$ m^2).

T (°C)	T (K)	d_{ap} (kg/m^3)	ε_0	c_B^0 (kmol/m^3)	t_0 (min)	kS_i ($\times 10^6$ kmol/min)
825	1098	1850	0.304	2.775	0.9	1.75
825	1098	1950	0.267	2.925	0.8	1.75
825	1098	2050	0.229	3.075	0.9	1.75
850	1123	1850	0.304	2.775	1.0	2.35
850	1123	1950	0.267	2.925	0.8	2.35
850	1123	2050	0.229	3.075	1.0	2.35
875	1148	1850	0.304	2.775	1.0	3.1
875	1148	1950	0.267	2.925	0.9	3.1
875	1148	2050	0.229	3.075	0.8	3.1
900	1173	1850	0.304	2.775	0.9	4.1
900	1173	1950	0.267	2.925	1.0	4.1
900	1173	2050	0.229	3.075	0.8	4.1
925	1198	1850	0.304	2.775	0.9	5.2
925	1198	1950	0.267	2.925	0.9	5.2
925	1198	2050	0.229	3.075	0.8	5.2
950	1223	1850	0.304	2.775	1.1	6.7
950	1223	1950	0.267	2.925	0.8	6.7
950	1223	2050	0.229	3.075	0.9	6.7

experiments performed, in order to attempt to correlate these, in each case trying different values of D_e.

Since the experiments were conducted with $c_Q^G = 0$, Eq. (5) adopted the following form:

$$t = t_0 + \frac{3S_S L c_B^0}{2kS_i}[1 - (1 - X)^{2/3}] + \frac{L^2 c_B^0 X^2}{8D_e K_C} \quad (10)$$

Using this equation and trying different diffusivity (D_e) values did not provide satisfactory results, because the resulting plots did not fit well the experimental data in the entire range of test temperatures.

As a result, Eq. (4) was only applied to experimental data corresponding to the highest values of X, at which the test piece shell in which the calcite had decomposed might already be sufficiently thick for the carbon dioxide diffusion step through it to affect the overall process rate, applying Eq. (9) only to the experimental data corresponding to the lowest conversion range. When this approach was adopted, very satisfactory results were obtained, which are detailed below.

Eq. (4) was analytically integrated from initial boundary conditions ($X = X_{02}$, $t = t_{02}$), setting $c_Q^G = 0$, which yielded:

$$t = t_{02} + \frac{3S_S L c_B^0}{2kS_i}[(1 - X_{02})^{2/3} - (1 - X)^{2/3}] + \frac{L^2 c_B^0}{4D_e K_C}\left[\frac{X^2}{2} - \frac{X_{02}^2}{2}\right] \quad (11)$$

where X_{02} and t_{02} must be a pair of values corresponding to the curve obtained for application of Eq. (9) to the same operating conditions.

The values of X_{02} and of t_{02}, as well as the corresponding value of D_e, were determined by trial and error in each experiment, applying Eq. (11), starting with a pair of X and t values obtained from Eq. (9) applied to the corresponding operating conditions. Using Eq. (11), different values of D_e and different corresponding pairs of values of $X - t$ obtained from Eq. (9) were tried until the best fit of Eq. (11) to the last section of the experimental data plot was found. These values were confirmed when Eq. (4), setting $c_Q^G = 0$, was integrated with the fourth-order Runge–Kutta method from initial boundary conditions ($X = X_{02}$, $t = t_{02}$), trying different values of D_e and different corresponding pairs of values of $X - t$ obtained from Eq. (9) until the best fit was found.

The starting pair of X and t values used in the trial-and-error procedure must be located, roughly, in the region in which it was visually observed that Eq. (9) ceased to fit the experimental data.

Table 4 presents the values of X_{02} and of t_{02}, as well as those of D_e resulting from the best fits obtained on applying Eq. (11) to the second sections of the experimental data plots. The table also gives the values of K_C used in each case, calculated from

Table 4
Values of X_{02}, t_{02}, and D_e obtained in the best fits with Eq. (11); ($L = 0.007$ m; $S_S = 0.00125$ m^2).

T (°C)	ε_0	t_{02} (min)	X_{02}	D_e (m^2/min)	K_c (kmol/m^3)
825	0.304	9.50	0.555	0.00030	0.0039
825	0.267	10.7	0.580	0.00019	0.0039
825	0.229	11.00	0.580	0.000115	0.0039
850	0.304	9.50	0.700	0.00033	0.00534
850	0.267	9.50	0.680	0.00021	0.00534
850	0.229	9.68	0.652	0.00013	0.00534
875	0.304	8.10	0.754	0.00037	0.0081
875	0.267	8.00	0.729	0.000235	0.0081
875	0.229	8.20	0.716	0.000145	0.0081
900	0.304	6.95	0.816	0.00041	0.0114
900	0.267	7.00	0.757	0.00026	0.0114
900	0.229	8.00	0.780	0.00016	0.0114
925	0.304	6.00	0.850	0.00046	0.0155
925	0.267	6.50	0.880	0.00029	0.0155
925	0.229	7.50	0.910	0.00018	0.0155
950	0.304	5.25	0.886	0.00051	0.0215
950	0.267	5.76	0.945	0.00032	0.0215
950	0.229	6.25	0.963	0.00019	0.0215

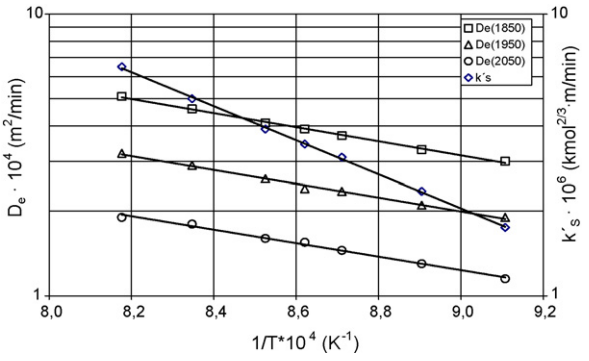

Fig. 6. Variation of kinetic parameters D_e and kS_i of Eqs. (9) and (11) with temperature (K).

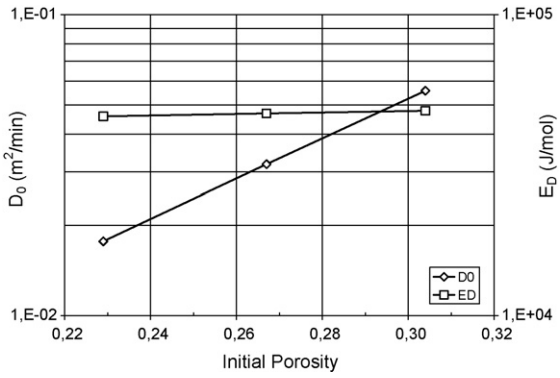

Fig. 7. Variation of D_0 and of the apparent activation energy E_D of Eqs. (15)–(17) with ε_0.

the equation:

$$K_C = \frac{P_Q^0}{RT} \tag{12}$$

where K_C is the equilibrium constant (kmol/m^3) of the reversible chemical reaction of calcium carbonate thermal decomposition, R is the gas constant (0.082 atm m^3 $kmol^{-1}$ K^{-1}) and P_Q^0 is the thermal dissociation pressure of calcium carbonate (in atm) at temperature T (in K), calculated from the equation[19,20]:

$$P_Q^0 = (1.3158 \times 10^{-3})(10^{10.4022-8792.3/T}) \tag{13}$$

The magnitude of the values obtained for D_e in the range of temperatures 825–900 °C (Table 4) is of the same order as that of the values determined experimentally in the study of black core oxidation, with air, during the firing of ceramic ware of an analogous nature to that of the test pieces used in this study, in the same temperature range.[11]

In that study, in which the oxidation process of carbon (contained in the black core) was solely controlled by molecular counter diffusion between O_2 (reactant) and CO_2 (carbon oxidation product) through the shell of the oxidised body, operating at temperatures of 850 °C (1123 K) and 900 °C (1173 K), the values 1.907×10^{-2} cm^2/s (1.14×10^{-4} m^2/min) and 2.23×10^{-2} cm^2/s (1.34×10^{-4} m^2/min) were respectively obtained for effective diffusivity in test pieces whose porosity, after firing, was 0.256. Those values are practically of the same order as the values in Table 4 (1.3×10^{-4} and 1.60×10^{-4} m^2/min) at the same temperatures, in test pieces whose initial dry porosity was 0.229. Dry porosity usually being lower than fired porosity in bodies of the type studied here.

4.2.3. Variation of the rate constant (k) and the effective diffusivity (D_e) with temperature

Fig. 6 presents the plots, on semi-logarithmic coordinates, of the variation of the product (kS_i), which includes the kinetic constant of the direct reaction of the chemical step, as well as that of the diffusion coefficient D_e, for each of the three test piece bulk densities, versus the inverse of operating temperature, expressed in K.

The resulting plots display straight lines of negative slope which were fitted to Eq. (14) for the product (kS_i) and to Eqs. (15)–(17) for D_e in the test pieces with initial porosities of 0.304, 0.267, and 0.229, respectively.

$$kS_i = 0.866 \exp\left(-\frac{119689}{RT}\right) \tag{14}$$

$$D_e = 0.05583 \exp\left(-\frac{47835}{RT}\right) \quad (\varepsilon_0 = 0.304) \tag{15}$$

$$D_e = 0.0318 \exp\left(-\frac{46858}{RT}\right) \quad (\varepsilon_0 = 0.267) \tag{16}$$

$$D_e = 0.01767 exp\left(-\frac{45857}{RT}\right) \quad (\varepsilon_0 = 0.229) \tag{17}$$

The resulting apparent activation energy of the reaction chemical step, which was 119689 J/mol (Eq. (14)), is of the same order as the values proposed by some researchers[21] for calcium carbonate thermal decomposition (118,000 J/mol), though it is considerably lower than the value we found for the decomposition of isolated calcite particles of the same type as those used in this study[18] (175,000 J/mol).

4.2.4. Relationship between effective diffusivity and initial porosity of the test pieces

In the foregoing section, three equations were obtained that relate D_e to temperature, corresponding to the three initial test piece porosities tested, of the following form:

$$D_e = D_0 exp\left(-\frac{E_D}{RT}\right) \tag{18}$$

It may be observed that, in these equations, D_e and E_D decrease slightly when test piece initial porosity decreases.

With a view to having a single expression for D_e that was valid for any test piece bulk density within the range of bulk density values studied, the possibility was tested of relating the values of the pre-exponential factor D_0 and of the apparent activation energy E_D of these equations by empirical expressions that related these kinetic parameters to test piece initial porosity (ε_0). An acceptable alignment was obtained, using semi-logarithmic coordinates, as Fig. 7 show.

The following equations were obtained from the plots:

$$D_0 = 5.277 \times 10^{-4} \exp(15.34\,\varepsilon_0) \tag{19}$$

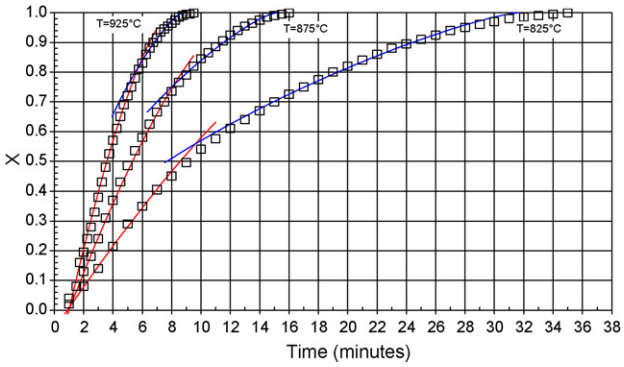

Fig. 8. Fit of the experimental data with Eq. (9) (red line) and (11) (blue line). d_{ap} = 1850 kg/m^3 (ε_0 = 0.304). T = 825, 875, and 925 °C.

$$E_D = 4.031 \times 10^4 \exp(0.563\,\varepsilon_0) \quad (20)$$

Substituting Eqs. (19) and (20) in Eq. (18) yielded a single expression representing the variation of D_e with temperature (T) and test piece initial porosity (ε_0), which was valid for the tested range of operating conditions, of the following form:

$$D_e = 5.277 \times 10^{-4} \exp(15.34\varepsilon_0) \exp\left[-\frac{4.031 \times 10^4\, exp(0.563\,\varepsilon_0)}{RT}\right] \quad (21)$$

4.2.5. Comparison between the experimental data and the values calculated from Eqs. (9) and (11): validity of the equations obtained for reproducing the experimental results

With a view to verifying the validity of Eqs. (9) and (11), obtained from the proposed kinetic model using the procedure described in Sections 4.2.1 and 4.2.2, the six studied operating temperatures and the three initial porosities were successively introduced into these equations, starting with the respective values of t_0 shown in Table 3 and switching from Eq. (9) to (11) for the corresponding t_{02} and X_{02} values detailed in Table 4. For each test temperature and initial porosity, the values of the kinetic parameters K_c, kS_i, and D_e were used, calculated from Eqs. (12) to (17), respectively, using the values L = 0.007 m, S_S = 0.00125 m^2, and c_B^0 equal to 2.775, 2.925 or 3.075 depending on the initial porosity of the test pieces used.

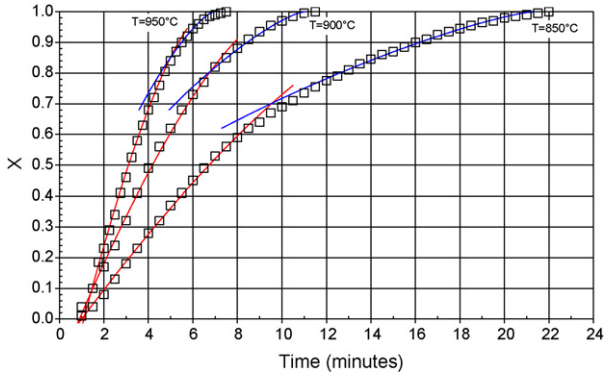

Fig. 9. Fit of the experimental data with Eq. (9) (red line) and (11) (blue line). d_{ap} = 1850 kg/m$_3$ (ε_0 = 0.304). T = 850, 900, and 950 °C.

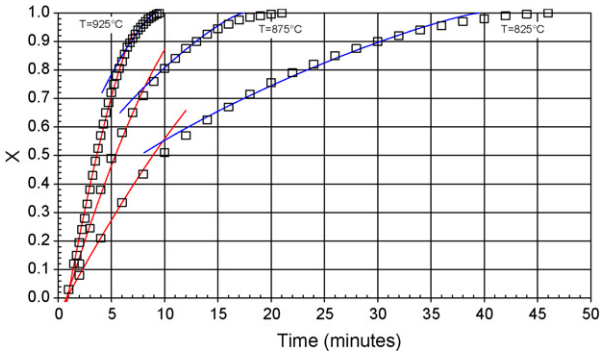

Fig. 10. Fit of the experimental data with Eqs. (9) (red line) and (11) (blue line). d_{ap} = 1950 kg/m^3 (ε_0 = 0.267). T = 825, 875, and 925 °C.

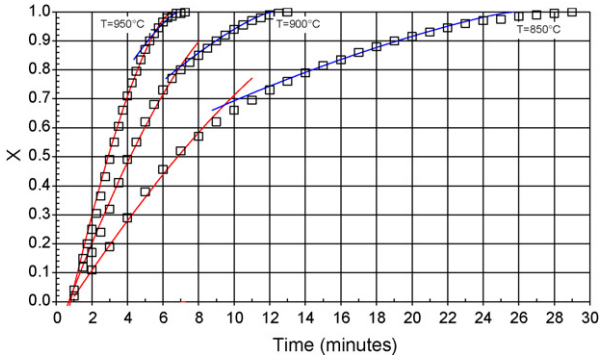

Fig. 11. Fit of the experimental data with Eqs. (9) (red line) and (11) (blue line). d_{ap} = 1950 kg/m^3 (ε_0 = 0.267). T = 850, 900, and 950 °C.

The $X = f(t)$ curves obtained in the form mentioned, have been plotted in Figs. 8–13 together with the corresponding experimental values.

Eq. (9) fits the experimental data very well, at all test temperatures and test piece initial porosities, for conversion degrees below 0.5 (first section of the red lines). As may be observed, the upper limit of the range of conversion degrees in which Eq. (9) can be applied increases when the operating temperature rises. Eq. (9) fits the 925 and 950 °C experimental data in practically the entire range of conversion degrees.

The curves corresponding to the best fits obtained with Eq. (11) (second section of the blue lines), also fit the experimental data very well, in the highest range of conversion degrees.

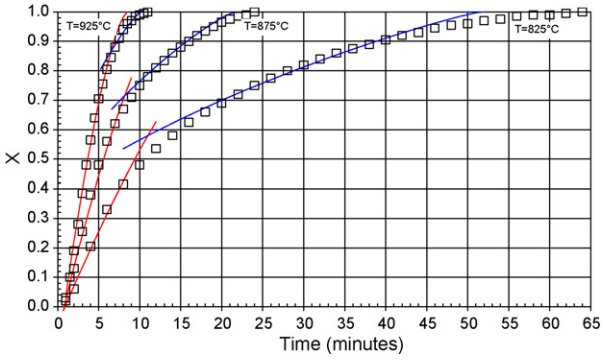

Fig. 12. Fit of the experimental data with Eqs. (9) (red line) and (11) (blue line). d_{ap} = 2050 kg/m^3 (ε_0 = 0.229). T = 825, 875, and 925 °C.

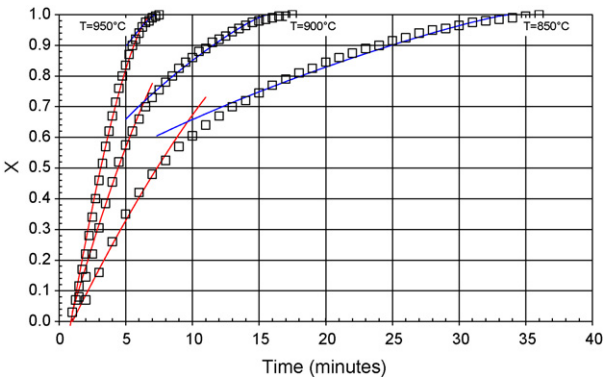

Fig. 13. Fit of the experimental data with Eqs. (9) (red line) and (11) (blue line). $d_{ap} = 2050\,kg/m^3$ ($\varepsilon_0 = 0.229$). $T = 850$, 900, and 950 °C.

The extent of this range decreases when operating temperature increases.

5. Conclusions

In this paper, the *Shrinking Core* kinetic model has been proposed to interpret the experimental results obtained in studying the thermal decomposition process, under isothermal conditions, of calcium carbonate as calcite particles with an average radius of 3.5 μm, uniformly distributed throughout the mass of test disks formed with the same type of natural raw materials mixture as that used in industrial practice to form the green bodies of white-firing earthenware wall tiles.

Starting with this kinetic model and using a rate equation proposed in a previous study for the $CaCO_3$ chemical decomposition step, in isolated calcite particles of the same nature as those used in this study, a differential equation has been deduced that relates the conversion degree of the calcium carbonate contained in the test pieces to the studied operating variables: time, temperature, and effective diffusivity (intimately related to the initial porosity of the studied test pieces).

Using this expression and assuming that, at the highest conversion degrees of the calcium carbonate contained in the studied test pieces, the overall process rate is simultaneously influenced by the chemical decomposition reaction step and by the diffusion step of the CO_2 resulting from this reaction through the porous structure of the reacted ceramic layer and that, at low conversion degrees, the overall process rate is only controlled by the chemical reaction step, the experimental data have been satisfactorily correlated. The equation proposed for each reaction period allows the experimental data, obtained under isothermal conditions in the tested range of operating conditions, to be reproduced with sufficient precision.

The CO_2 effective diffusion coefficients, obtained by fitting the experimental data with the proposed equations, are practically of the same order as those obtained previously in the study of carbon oxidation in black cores present in ceramic bodies of a similar nature to that of the bodies tested here, during the firing process. An expression has been obtained that relates the CO_2 effective diffusion coefficients to the initial porosity of the test pieces.

Acknowledgements

The authors thank the Instituto de la Mediana y Pequeña Empresa de Valencia (IMPIVA) of the Generalitat Valenciana for its financial help. They are also grateful for the support of FEDER funds from the European Union. Project reference IMIDIC/2007/102.

Appendix A.

A.1. Application of the Shrinking Unreacted Core kinetic model to the studied process

Applying this kinetic model, it is assumed that $CaCO_3$ (*B*) decomposition in the test pieces used, characterised as flat slabs of infinite width and length and finite thickness, occurs from the two slab outer surfaces inwards. In addition, it is also assumed that the two reaction interfaces are also flat, the solid being assumed to behave isotropically in relation to the chemical reaction, and that the $CaCO_3$ decomposition rate is sufficiently high to be able to assume that this reaction only occurs in two layers (flat in this case) of negligible thickness, located on either side of the piece parallel to the middle plane (reaction interfaces). Therefore, the thickness of each of the two layers [inert solid (I) + CaO (P)] that form is assumed to be uniform and identical on both sides of the piece (Fig. A.1).

It is also assumed that the CO_2 released at the reaction interfaces moves through pores of the regions of the piece where decomposition has already occurred, filling them completely. At temperatures above 897 °C, in the reaction interfaces, where carbon dioxide pressure must be equal to the $CaCO_3$ decomposition pressure at reaction interface temperature ($P^0_{CO_2}$), CO_2 pressure can become even higher than the total pressure at the solid–gas interface and in the gas phase. As a result, above this temperature, CO_2 may move by a laminar flow mechanism through the reacted layer of the piece, as well as by the diffusion mechanism.

A.2. Overall rate equation

In order to obtain a representative rate equation of the overall process, it is necessary to take into account the rate at which the chemical reaction step of $CaCO_3$ decomposition unfolds and the rate of the two transport steps of the CO_2 resulting from

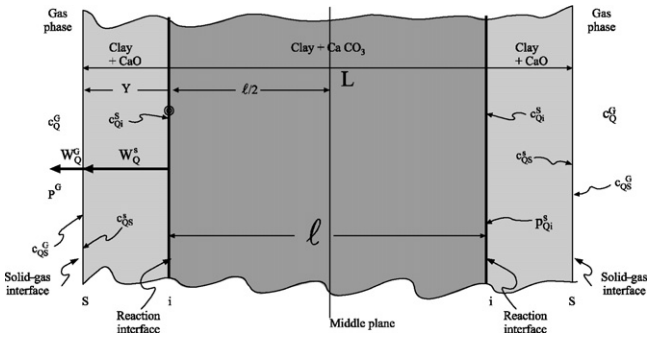

Fig. A.1. Test piece cross-section.

this reaction, which occur simultaneously and consecutively: (a) movement of CO_2, from the reaction interface, through the [inert solid + CaO] layer, to the solid–gas interface and (b) turbulent transport of CO_2 from that interface into the gas phase. The inert solid mentioned is assumed to consist of the materials (other than calcite) initially used to form the ceramic body, which have lost some constituents during thermal treatment.

A.2.1. $CaCO_3$ chemical reaction rate

It is assumed that the chemical reaction unfolds at the two reaction interfaces illustrated in Fig. A.1, as previously described.

It was experimentally established that the rate at which the calcium carbonate chemical decomposition step unfolds, in the calcite particles contained in the raw materials mixture used to form the test pieces in this study, can be represented by Eq. (3).

Assuming that this equation could also be applied to the decomposition of the $CaCO_3$, uniformly and homogenously distributed throughout the mass of the test pieces, one obtains:

$$R_B = \nu_B(1-X)^{1/3} S_i k \left(1 - \frac{C^s_{Qi}}{K_C}\right) \quad (A.1)$$

where all the variables have already been defined.

A.2.2. CO_2 transport from the reaction interfaces to the solid–gas interface in the test piece

With regard to CO_2 movement through the inert solid layer (Fig. A.1), two possibilities are considered: (a) diffusion transport (at operating temperatures below 897 °C); and (b) transport by laminar or viscous flow (at temperatures above 897 °C), in accordance with what has been set out in the last paragraph of Section A.1. At temperatures above 897 °C, CO_2 transport is likely to occur by both mechanisms, the latter predominating as the temperature rises because the decomposition pressure (CO_2 pressure at the reaction interface) increases considerably with temperature.

In order to express the corresponding rate equation, in principle, only one half of the laminar test piece (from the middle plane to the outer surface of the test piece) is considered, the resulting expression then being applied to both halves.

For diffusion transport in a quasi-steady-state regime, taking into account that a slab of parallel faces is involved, the following equation is obtained[20]:

$$\frac{(W^S_Q)_{dif}}{2} = S_S \frac{D_Y}{Y}(c^S_{Qi} - c^S_{QS}) \quad (\text{kmol Q/min}) \quad (A.2)$$

where $(W^S_Q)_{dif}/2$ is the molar flow of Q (through the [inert solid + CaO] layer corresponding to the considered slab half), S_S is the piece cross-section parallel to the two flat faces that bound the slab; $c^S_{Qi} = P^S_{Qi}/RT$, where $P^S_{Qi} = P^0_{CO_2}$ (calculated at the reaction interface temperature); c^S_{QS} is the concentration of Q at the solid–gas interface, on the solid side, and D_Y is the intergrain diffusivity of CO_2 through the reacted layer of thickness Y (see Fig. A.1).

For transport by viscous flow, when the system temperature is higher than 897 °C ($P^0_Q > 1$ atm abs.), an equation can be obtained of the following form[20]:

$$\frac{(W^S_Q)_{vf}}{2} = \frac{c^S_{Qi} - c^S_{QS}}{2\mu_Q Y/S_S k_p RT(c^S_{Qi} + c^S_{QS})} \quad (\text{kmol Q/min}) \quad (A.3)$$

where $(W^S_Q)_{vf}/2$ is the molar flow of Q (through the CaO layer corresponding to the considered slab half) solely due to the viscous flow mechanism, μ_Q is the viscosity of Q (kg/m min), k_p is the permeability of the reacted layer of the test piece (m^2), and R is the gas constant ($R = 0.082$ atm m^3 $kmol^{-1}$ K^{-1}).

At $T > 897$ °C, CO_2 viscous flow is probably accompanied by CO_2 diffusion transport, both phenomena developing in a parallel manner. In this case, the total CO_2 flow that moves from the reaction interface to the solid–gas interface, through the [inert solid + CaO] layer corresponding to one of two slab halves being considered (Fig. A.1), is equal to the sum of the flow rates corresponding to transport by viscous flow and by intergrain diffusion. Eqs. (A.2) and (A.3) yield:

$$\frac{W^S_Q}{2} = \frac{(W^S_Q)_{fv}}{2} + \frac{(W^S_Q)_{dif}}{2} = \frac{c^S_{Qi} - c^S_{QS}}{2Y/(S_S[(k_p/\mu_Q)RT(c^S_{Qi} + c^S_{QS}) + 2D_Y])} \quad (A.4)$$

If one sets

$$\left(\frac{k_p}{\mu_Q}\right) RT(c^S_{Qi} + c^S_{QS}) + 2D_Y = 2D_e \quad (A.5)$$

in Eq. (A.4), this becomes:

$$\frac{W^S_Q}{2} = S_S \frac{D_e}{Y}(c^S_{Qi} - c^S_{QS}) \quad (\text{kmol Q/min}) \quad (A.6)$$

In accordance with Eq. (5), D_e (overall effective diffusivity stemming from the two mechanisms considered) must be larger than the diffusion coefficient D_Y, which only corresponds to the intergrain diffusion mechanism, at working temperatures above 897 °C.

A.2.3. Turbulent transport of CO_2 from the solid–gas interface into the gas

If one half of the slab is considered, the corresponding flow rate equation will be of the form:

$$\frac{W^G_Q}{2} = S_S k_G(c^G_{QS} - c^G_Q) \quad (\text{kmol Q/min}) \quad (A.7)$$

where k_G is the corresponding mass transfer coefficient of CO_2 (m/min).

A.2.4. Overall rate equation

The relationship that exists between the reaction rate (decomposition) of calcium carbonate (B) and the CO_2 (Q) formation

rate is given by the expression:

$$\frac{R_Q}{\nu_Q} = \frac{R_B}{\nu_B} \tag{A.8}$$

On the other hand, since all the CO_2 that is released in the decomposition reaction needs to move to the outside of the particle, in a quasi-steady-state regime, the following must be obeyed for any value of t throughout the process:

$$R_Q = W_Q^S = W_Q^G \tag{A.9}$$

Solving for R_B, Eqs. (A.8) and (A.9) yield:

$$R_B = R_Q\left(\frac{\nu_B}{\nu_Q}\right) = W_Q^S\left(\frac{\nu_B}{\nu_Q}\right) = W_Q^G\left(\frac{\nu_B}{\nu_Q}\right)$$

Taking into account the values of the stoichiometric coefficients in reaction scheme (1) ($-\nu_B = \nu_Q = 1$), this gives:

$$-R_B = R_Q = W_Q^S = W_Q^G \tag{A.10}$$

if a quasi-steady state is assumed.

Eqs. (A.10), (A.1), (A.6) and (A.7) yield:

$$-R_B = \frac{1 - c_{Qi}^S/K_C}{1/(kS_i(1-X)^{1/3})} = \frac{c_{Qi}^S/K_C - c_{QS}^S/K_C}{Y/(2S_S D_e K_C)} = \frac{c_{QS}^G/K_C - c_Q^G/K_C}{1/(2S_S k_G K_C)} \tag{A.11}$$

Regrouping terms, applying the property of proportions to the foregoing equation, and assuming that, in this case, $c_{QS}^S = c_{QS}^G$ (Fig. A.1) is obeyed, gives:

$$-R_B = \frac{1 - c_Q^G/K_C}{1/(kS_i(1-X)^{1/3}) + Y/(2S_S D_e K_C) + 1/(2S_S k_G K_C)} \tag{A.12}$$

From Fig. A.1, it is deduced that: $Y = (L - \ell)/2$

On the other hand: $X = (L - \ell)/L$ As a result:

$$X = \frac{2Y}{L} \quad \text{or also} \quad Y = \frac{LX}{2} \tag{A.13}$$

Eqs. (A.12) and (A.13) give:

$$-R_B = \frac{1 - c_Q^G/K_C}{(1/(kS_i(1-X)^{1/3})) + (LX/(4S_S D_e K_C)) + (1/(2S_S k_G K_C))} \tag{A.14}$$

which represents the overall process rate relating to component B ($CaCO_3$).

A.3. Correlation between the degree of transformation progress and reaction time

A.3.1. Balance of B

In the flat laminar disk being considered, it is assumed that $CaCO_3$ (B) is uniformly dispersed in an inert solid, in the form of small-sized particles (below 3.5 μm). Therefore, ρ_B (molar density of B) is expressed as the number of kmol of $CaCO_3$ (B) contained in a cubic metre of test disk.

Applying the law of conservation of matter to component B contained in a test disk, assuming the disk behaves as a discontinuous reaction system, and taking into account that a flat slab is involved, one obtains:

$$R_B = \frac{dN_B}{dt} = N_B^0\left(-\frac{dX}{dt}\right) = \rho_B^0 V_B^0\left(-\frac{dX}{dt}\right) = c_B^0 S_S L\left(-\frac{dX}{dt}\right) \tag{A.15}$$

where ρ_B^0 is the initial molar density of $CaCO_3$ in the test piece, taking into account that $\rho_B^0 = c_B^0$.

A.3.2. Correlation between the degree of reaction progress and t, under isothermal conditions

The differential equation that enables the degree of reaction progress to be related to t is obtained by setting the last member of Eq. (A.15), with changed sign, equal to the second member of Eq. (A.14). By operating, this gives:

$$\frac{dX}{dt} = \frac{1}{Lc_B^0}\left[\frac{1 - c_Q^G/K_C}{(S_S/(kS_i(1-X)^{1/3}) + (LX/4D_e K_C) + (1/2k_G K_C)}\right] \tag{A.16}$$

When the process unfolds under conditions such that the CO_2 turbulent transport step, from the solid–gas interface into the gas phase in contact with the test disk, unfolds much more quickly than the chemical reaction and CO_2 diffusion steps through the reacted layer, the third term of the denominator of the foregoing equation, representing the resistance opposed by this step, can be discarded, yielding:

$$\frac{dX}{dt} = \frac{1}{Lc_B^0}\left[\frac{1 - c_Q^G/K_C}{(S_S/(kS_i(1-X)^{1/3})) + (LX/4D_e K_C)}\right] \tag{A.17}$$

References

1. Smith AN. Investigations on the moisture expansion of porous ceramic bodies. *Trans Br Ceram Soc* 1955;**54**(5):300–18.
2. Sánchez E, García J, Sanz V, Ochandio E. Raw material selection criteria for the production of floor and wall tiles. *Tile Brick Int* 1990;**6**(4):15–21.
3. Amorós JL, Escardino A, Sanchez E, Zaera F. Stabilità delle dimensioni nelle piastrelle porose monocotte. *Ceram Inf* 1993;**324**:56–67.
4. Sánchez E, Garcıa-Ten J, Regueiro M. Materias para la industria cerámica española. Situación actual y perspectivas. *Bol Soc Esp Ceram Vidr* 2006;**45**(1):1–12.
5. Beltrán V, Sanchez E, García-Ten J, Ginés F. Materias primas empleadas en la fabricación de baldosas de pasta blanca en España. *Téc Cerám* 1996;**241**:114–28.
6. Todor DN. *Thermal analysis of minerals*. Tunbridge Wells: Abacus Press; 1976.
7. Amorós JL, Beltrán V, Blasco A, Enrique JE, Escardino A, Negre F, et al. *Defectos de fabricación de pavimentos y revestimientos cerámicos. [Castellón]*. AICE-Instituto de Tecnología Cerámica; 1991.
8. Fogler SH. *The elements of chemical reaction engineering*. New Jersey: Prentice-Hall; 1986. p. 532.
9. Perry RH, Chilton CH, Kirkpatrick SD. *Perry's: chemical engineersĭ handbook*. 6th ed. New York: McGraw-Hill; 1984. p. 4–10.
10. Negre F, Escardino A, Amorós JL, Barba A. Oxidation of black core during the firing of ceramic ware—2. Process kinetics. *Br Ceram Trans J* 1992;**91**:5–11.
11. Escardino A, Barba A, Blasco A, Negre F. Oxidation of black core during firing of ceramic ware: 4. Relationship between effective diffusivity

of oxygen through oxidised layer and properties characterising its porous structure. *Br Ceram Trans* 1995;**94**(3):103–8.
12. Doraiswamy LK, Sharma MM. *Heterogeneous reactions: analysis, examples, and reactor design: volume 1: gas–solid and solid–solid reactions*. New York: John Wiley and Sons; 1984. p. 450–6.
13. Levenspiel O. *El Omnilibro de los Reactores Químicos*. Barcelona: Reverté; 1986. pp. 55.3–4.
14. Scott Fogler H. *Elements of chemical reaction engineering*. New Jersey: Prentice-Hall Inc.; 1986. p. 561–2.
15. Satterfield CN. *Mass transfer in heterogeneous catalyst*. Cambridge, MA: MIT Press; 1972.
16. Orts Tarí MJ. Sinterización de piezas de pavimento gresificado. PhD dissertation. Castellón: Universitat de València, Departament dïEnginiería Química; 1991.
17. Escardino A, Amorós JL, Orts MJ, Beltrán V. Influence of pressing variables on air permeability of fired floor tile bodies. In: Carty WM, Sinton CW, editors. *Science of whitewares II*. Westerville: ACERS; 2000. p. 309–18.
18. Escardino A, García-Ten J, Feliu C. Kinetic study of calcite particle (powder) thermal decomposition: Part I. *J Eur Ceram Soc* 2008;**28**:3011–20.
19. Hill KJ, Winter ERS. Thermal dissociation pressure of calcium carbonate. *J Phys Chem* 1956;**60**:1361-1362.
20. Garcia-Ten J. Descomposición, durante la cocción, del carbonato cálcico contenido en el soporte crudo de los azulejos. PhD dissertation. Castellón: Universitat Jaume I. Departament dïEnginiería Química; 2005.
21. Rajeswara Rao T. Kinetics of calcium carbonate decomposition. *Chem Eng Technol* 1996;**19**:373–7.